Am J Cancer Res 2024;14(11):5230-5250
www.ajcr.us /ISSN:2156-6976/ajcr0158807

*Original Article*

# Integration of bioinformatics analysis reveals ZNF248 as a potential prognostic and immunotherapeutic biomarker for LIHC: machine learning and experimental evidence

Lifang Weng, Zhicheng Cheng, Zhisong Qiu, Jin Shi, Libin Chen, Chunsheng He, Lijuan Wang, Feng Jin

*Department of Gastroenterology, Cangshan Hospital, The 900Th Hospital of Joint Logistics Support Force of Chinese People's Liberation Army, Fuzhou, Fujian, The People's Republic of China*

Received June 27, 2024; Accepted October 27, 2024; Epub November 15, 2024; Published November 30, 2024

**Abstract:** Liver hepatocellular carcinoma (LIHC) is a major contributor to cancer-related mortality worldwide, posing substantial diagnostic and therapeutic challenges. Although zinc finger proteins (ZNFs) are known to play a role in LIHC, the specific function of ZNF248 remains poorly understood. In this study, we analyzed genomic and clinical data from The Cancer Genome Atlas (TCGA) to elucidate the role of ZNF248 through differential expression analysis, bioenrichment, immune response correlation, and drug sensitivity evaluation. Machine learning was employed to identify prognostic signatures derived from ZNF248, which were further validated using Receiver Operating Characteristic (ROC) analysis. Functional assays, including Western blot and rescue experiments, were performed to assess the impact of ZNF248 on the PI3K/AKT signaling pathway. Our results demonstrate that ZNF248 is significantly overexpressed in LIHC patients and is associated with poor prognosis. Bioenrichment analysis revealed activation of oncogenic pathways, and elevated ZNF248 expression correlated with increased immune cell infiltration and enhanced immune scores, thereby influencing both immunotherapy response and drug sensitivity. Functional assays further confirmed that ZNF248 promotes LIHC progression and invasion, while silencing ZNF248 inhibited the PI3K/AKT pathway - a phenomenon reversible by the AKT activator SC79. These findings suggest that ZNF248 contributes to LIHC progression through the PI3K/AKT pathway and may represent a novel immunotherapeutic target and prognostic biomarker for LIHC.

**Keywords:** ZNF248, LIHC, immune infiltration, immunotherapy, prognostic indicator, machine learning

## Introduction

Liver cancer is one of the most significant global health challenges, consistently ranking among the leading causes of cancer-related deaths [1]. Liver hepatocellular carcinoma (LIHC) is the predominant subtype, accounting for approximately 90% of primary liver cancers [2]. Current therapeutic approaches for LIHC include surgical resection, organ transplantation, local radiotherapy, and drug therapy [3]. Notably, hepatectomy is considered the standard radical treatment, but only a small proportion of patients, primarily those in early stages, are eligible for this procedure [4]. The lack of early biomarkers for LIHC often results in diagnoses at intermediate to advanced stages, leading to poor prognosis and significantly impacting global health [3]. Thus, identifying new diagnostic and therapeutic targets is crucial for improving LIHC patient survival rates.

Zinc Finger Protein 248 (ZNF248), a member of the zinc finger protein family, is located on chromosome 10p11 and encodes a 579-amino acid protein with a predicted molecular weight of 67.1 kDa [5]. ZNF248 contains a Kruppel-related box (KRAB) domain, functioning as a regulatory transcription factor [5]. Zuo et al. identified ZNF248 as a broad-spectrum long interspersed nuclear element-1 (LINE-1)-binding agent [6]. LINE-1 retrotransposons are mobile genetic elements that may reduce tumor suppression in somatic cells and are implicated

https://doi.org/10.62347/CDUS5096

in LIHC pathogenesis and progression [7]. Although the physiological function of ZNF248 is not well-studied, the ZNF family has been shown to play essential roles in various diseases, including cancer [8]. He et al. found that overexpression of ZNF384 in LIHC tissues was associated with tumor recurrence and promoted LIHC cell proliferation by upregulating cell-cycle protein D1 [9]. Xie et al. revealed that knockdown of ZNF233 inhibited LIHC cell proliferation and tumorigenesis [10]. Wang et al. observed that ZNF-148 could induce heat shock cell death mediated by the miR-335/SOD2/ROS axis, promoting breast cancer progression. However, no studies have yet explored the function of ZNF248 in LIHC [11].

Bioinformatic analysis significantly contributes to understanding disease pathogenesis, identifying diagnostic markers, and discovering therapeutic targets through the examination of genomic, transcriptomic, and proteomic data [12]. This study aimed to apply bioinformatic analysis to determine the biological role of ZNF248 in LIHC. Using data from The Cancer Genome Atlas (TCGA), we conducted bioenrichment, immunological correlation analysis, genomic characterization, and drug sensitivity analysis. We also modeled the prognostic risk associated with ZNF248. Ultimately, we identified ZNF248 as a novel immunotherapeutic biomarker for the LIHC immune microenvironment. Our study provides promising insights for the diagnosis and treatment of LIHC.

## Method

### *Public data acquisition*

Transcriptomic and clinical characterization data used in this research were obtained from The Cancer Genome Atlas (TCGA) database (https://tcgadata.nci.nih.gov/). For subsequent analyses, we retrieved the original expression profiles (represented as STAR counts) of LIHC patients and converted them into a combinatorial matrix (depicted as TPM). Survival and clinical information of the patients were gathered from the TCGA-LIHC bcr-xml file. The harmonized and standardized pan-cancer dataset was sourced from the University of California Santa Cruz (UCSC) database (https://xenabrowser.net/): TCGA Pan-Cancer (PANCAN, N = 10535, G = 60499). From this dataset, we extracted the expression data of the ENSG00000198105 (ZNF248) gene in individual samples and screened samples derived from Solid Tissue Normal, Primary Blood Derived Cancer - Peripheral Blood, and Primary Tumor. Samples with expression levels of 0 were excluded, and the data were normalized by log2 (x+1). Ultimately, expression data for 26 cancer types were acquired, excluding cancer types with fewer than three samples. Immunohistochemistry images for LIHC were obtained from the Human Protein Atlas (HPA) database.

### *Differential analysis*

Differentially expressed genes (DEGs) were identified using the limma package in the R environment. Genes with a $P$ value < 0.05 and |Log2 fold-change (log2FC)| ≥ 0.585 were defined as DEGs. Volcano plots were generated using the ggplot2 V3.3.5 package in R.

### *Bioenrichment*

Gene Set Enrichment Analysis (GSEA) (https://www.bioincloud.tech/standalone-task-ui/anzy_GSEA_analysis_hallmark) was employed to conduct enrichment analysis on known gene sets, such as the Hallmark gene set, to assess whether these genes displayed statistically significant and consistent differences between two biological states [13]. Single-sample GSEA (ssGSEA) was used to quantify gene set enrichment by calculating the degree of expression of the gene set in each sample [14]. Overlapping DEGs were analyzed for Gene Ontology (GO) pathway functional enrichment using the Clusterprofiler package in R, including GO terms such as biological process (BP), cellular component (CC), and molecular function (MF) [15, 16].

### *Immune-related analysis*

Immune cell infiltration in the tumor microenvironment (TME) of LIHC in the ZNF248 high and low expression groups was evaluated using seven algorithms: CIBERSORT, MCPcounter, xCell, EPIC, TIMER, QUANTISEQ, and ESTIMATE [17-22]. Tumor immune dysfunction and exclusion (TIDE) and immunophenoscore (IPS) scores are good predictors of tumor immunotherapy response rates, particularly for anti-CTLA-4 and anti-PD-1 antibody responses [23, 24]. Thus, using the TIDE (http://tide.dfci.harvard.edu/) and IPS algorithms, we evaluated

the potential of ZNF248 in predicting immunotherapy responses in LIHC patients. Lower TIDE scores and higher IPS scores indicate better immunotherapy responses.

*Genomic characterization*

The Tumor Stem Cell Index (mDNAsi, mRNAsi) scores in the TCGA-LIHC project were generated through a quantitative study of stemness in tumor samples using a previously published machine learning algorithm (OCLR, One Class Linear Regression) [25]. Microsatellite instability (MSI) and tumor mutation burden (TMB) are essential immunotherapy biomarkers [26]. We downloaded TMB and MSI scores for ZNF248 from the TCGA database. Mutation profiles of ZNF248 were also analyzed and visualized using TCGA data. Drug-gene interactions and potential drug accessibility genes were investigated using the Drug-Gene Interaction database (DGIdb) (https://old.dgidb.org/search_categories).

*Drug sensitivity analysis*

Using the CellMiner database (http://discover.nci.nih.gov/cellminer/), RNA-seq expression profiles and National Cancer Institute (NCI) - 60 chemical activity data were downloaded to conduct a drug sensitivity study of ZNF248 [27]. The study involved FDA-approved or clinically tested drugs such as Dacomitinib, Cabozantinib, and Pentostatin. The "impute", "limma", "ggplot2", and "ggpubr" R packages were utilized.

*Nomogram*

A nomogram incorporating age, gender, TNM stage, and ZNF248 expression was constructed using the R "rms" and "survival" packages [28]. The nomograms forecasted the 1-, 3-, and 5-year overall survival of patients, and calibration curves were developed to evaluate their accuracy.

*Weighted gene co-expression network analysis (WGCNA)*

WGCNA was used to examine gene expression patterns in patient samples [29]. Following data preparation, the power function converted the correlation matrix into an adjacency matrix. The pickSoftThreshold() function analyzed network architecture to determine correlation values for different soft thresholds. The co-expression network was constructed based on the optimal soft thresholds, and the gene clustering tree was drawn. Similar modules were merged and visualized.

*Identification of prognosis signature based on machine learning*

Multivariate Cox regression analysis, using the R "survival" package, determined whether clinical characteristics such as gender, age, tumor stage, and ZNF248 expression could be independent survival predictors for LIHC patients. LIHC patients from the TCGA database served as the training cohort. A machine-learning prognostic model, employing Least Absolute Shrinkage and Selection Operator (LASSO) logistic regression, screened for molecules significantly associated with LIHC patient survival [30]. Multivariate Cox regression analysis was conducted on the genes in the feature set. The prognostic feature formula was determined as: "Risk score = Expression of A * Coef A + Expression of B * Coef B + ... + Expression of X * Coef X". The Kaplan-Meier (K-M) method was applied for prognostic survival analysis. The model's performance was evaluated using the Receiver Operating Characteristic (ROC) curve, with an AUC value > 0.7 indicating superior performance [31]. The GSE76427 dataset was used as an external validation cohort.

*Cell culture and transfection*

The hepatocellular carcinoma (HCC) cell lines, including PLC/PRF/5, Huh-7, MHCC-LM3, SNU-449, HepG2, MHCC97H, and Hep3B, along with human normal hepatocytes (LO-2), were cultured in Dulbecco's Modified Eagle's Medium (DMEM) or RPMI Medium 1640, both sourced from Gibco, supplemented with 10% fetal bovine serum (FBS). These cultures were maintained at 37°C in a 5% $CO_2$ atmosphere. For gene silencing, specific small interfering RNAs (siRNAs) targeting ZNF248 were obtained from RIBOBIO (Guangdong, China). The siRNA sequences employed are detailed in Table S1. A non-targeting RNA duplex served as the negative control (NC), ensuring it had no homology to any sequences within the human genome. Transfections were carried out using Lipofectamine® 3000 Transfection Reagent

(Invitrogen), strictly following the manufacturer's instructions.

*RNA isolation and reverse transcription quantitative polymerase chain reaction (RT-qPCR) procedure*

Total RNA was isolated from various hepatocellular carcinoma (HCC) cell lines using Trizol reagent (Takara, Japan). This RNA was then reverse transcribed to cDNA utilizing the PrimeScript RT Reagent Kit (Takara, Japan), adhering to the manufacturer's protocols. Gene expression analysis was conducted via RT-qPCR using TB Green Premix Ex Taq (Takara, Japan). The PCR primers, synthesized by Tsingke (Beijing, China), are detailed in Table S1. The PCR conditions involved an initial denaturation at 95°C for 5 minutes, followed by 40 cycles of a three-step PCR process (95°C for 40 seconds, 60°C for 50 seconds, and 72°C for 30 seconds). Primers were designed and supplied by Invitrogen. Gene expression data were quantitatively analyzed using the 2-ΔΔCT method, as referenced [32].

*CCK-8 assay*

For the CCK-8 assay, we seeded cells at a density of 5,000 cells per well in 96-well plates. After 24 hours, cells were treated with 10 μL of CCK-8 reagent per well. Cell viability was subsequently assessed at 24, 48, and 72-hour intervals using a microplate reader (Molecular Devices, Rockford, IL, USA). The absorbance was measured at an optical density of 460 nm to determine cell proliferation rates.

*Colony formation assay*

For the colony formation assay, Huh-7 and MHCC97H cells were plated at a density of 500 cells per well in six-well plates. The cells were cultured under standard conditions at 37°C and 5% $CO_2$ for two weeks to allow colony development. Following the incubation period, the colonies were fixed using 4% formaldehyde and subsequently stained with 0.2% crystal violet at room temperature for clear visualization. Representative colonies were then photographed and quantified to assess the clonogenic ability of the cells.

*5-ethynyl-2'-deoxyuridine (EdU) assay*

To assess cell proliferation, we utilized the 5-ethynyl-2'-deoxyuridine (EdU) assay, following the protocols provided by the BeyoClick™ EdU Cell Proliferation Kit with Alexa Fluor 555. Cells were plated at a density of 20,000 cells per well in an 8-well slide and incubated with 50 μmol/L EdU (dilution 1:1000) for 12 hours to incorporate the EdU into actively dividing cells. Post-incubation, cells were fixed with 4% formaldehyde at 37°C for 20 minutes, followed by permeabilization with 0.5% Triton X-100 at the same temperature. We then added 100 μL of Apollo reaction cocktail to the cells and incubated them in the dark for 30 minutes. After several washes with PBS, the nuclei were stained with 4',6-diamidino-2-phenylindole (DAPI) at 37°C for 20 minutes. The EdU-labeled cells were visualized using a laser scanning confocal microscope (Leica SP8). Quantification was done by normalizing the number of EdU-positive cells to the total number of DAPI-stained cells.

*Transwell migration and invasion assays*

We conducted migration assays using Matrigel-free transwell chambers (Corning, USA), and invasion assays were performed using chambers pre-coated with Matrigel (BD Biosciences). Cells were seeded into the upper chamber of a transwell setup (BD Biosciences, Franklin Lakes, NJ) at a concentration of 2 × 10^5 cells/ml. The cells were incubated for 48 hours at 37°C. Post-incubation, cells remaining on the upper surface of the membrane were gently removed. Cells that migrated or invaded to the bottom of the membrane were fixed with 4% paraformaldehyde for 10 minutes. Subsequently, the cells were stained with crystal violet (Beyotime, China) for 5 minutes for visualization. The stained cells were then counted under a microscope to assess migration and invasion capabilities.

*Western blot*

Protein expression levels were determined using Western blot analysis. Total protein was extracted from clinical samples or cell lines using RIPA lysis buffer (Beyotime) with 1% PMSF (Beyotime). Protein quantification was performed using a BCA kit. Proteins were separated by 10-12% SDS-PAGE and transferred to a PVDF membrane (Millipore, USA). The membrane was blocked with 5% skimmed milk for 1 hour at room temperature and incubated with primary antibodies overnight at 4°C. Afterward, secondary antibodies were applied for 1 hour

at room temperature. Protein visualization was achieved using an ECL kit (SeraCare, USA) and imaged with a Bio-Rad ChemiDoc Touch system (Bio-Rad Laboratories, USA). Band intensities were analyzed using Image Lab software (NIH, USA). GAPDH and β-tubulin served as internal controls. Details of the antibodies are in Table S2.

*Statistical analysis*

All statistical analyses were performed using R software. The statistical threshold for comparing *P* values was 0.05.

## Results

*Pan-cancer analysis of ZNF248 and its clinical role in LIHC*

According to TCGA data, ZNF248 exhibited an aberrant expression pattern in multiple cancers, suggesting its influential role in cancer development (**Figure 1A**). Significance of difference analysis revealed that ZNF248 expression levels were significantly higher in 10 tumor tissues compared to normal control tissues: LUAD (Tumor: 2.38 ± 0.51, Normal: 2.27 ± 0.38, P = 0.03), STES (Tumor: 2.38 ± 0.55, Normal: 2.17 ± 0.83, P = 0.02), KIRP (Tumor: 2.71 ± 0.79, Normal: 2.45 ± 0.35, P = 4.8e-4), KIPAN (Tumor: 2.84 ± 0.77, Normal: 2.45 ± 0.35, P = 1.6e-11), COAD (Tumor: 2.21 ± 0.39, Normal: 2.07 ± 0.57, P = 7.2e-3), STAD (Tumor: 2.38 ± 0.57, Normal: 2.14 ± 0.85, P = 0.02), KIRC (Tumor: 3.04 ± 0.67, Normal: 2.45 ± 0.35, P = 2.4e-24), LIHC (Tumor: 1.44 ± 0.54, Normal: 0.78 ± 0.23, P = 2.2e-17), PCPG (Tumor: 3.01 ± 0.55, Normal: 2.06 ± 0.49, P = 0.01), CHOL (Tumor: 2.27 ± 0.48, Normal: 1.05 ± 0.23, P = 2.7e-8). Immunohistochemistry results from the HPA database further showed that ZNF248 protein expression in LIHC tissues was higher than in normal tissues (**Figure 1B**). Additionally, we investigated the prognostic role of ZNF248 in LIHC. The results indicated that high ZNF248 expression might be associated with poorer prognosis in LIHC patients, affecting overall survival (OS) and progression-free survival (PFS) in the TCGA cohort (**Figure 1C**, **1D**). COX regression analysis identified ZNF248 as an independent risk factor for LIHC (**Figure 1E**). Further exploration of the clinical relevance of ZNF248 in LIHC patients revealed significantly elevated ZNF248 expression in female patients, those aged ≤ 65, and patients with TNM Stage III/IV (**Figure 1F-H**).

*ZNF248 exerts a wide biological regulatory effect in LIHC*

Patients were divided into two groups based on ZNF248 expression levels low- and high-expression and differential analysis was conducted. There were 1075 upregulated and 263 downregulated DEGs between the high and low ZNF248 expression groups (**Figure 2A**). GSEA of Hallmark pathways identified a positive correlation between ZNF248 expression and pathways like G2M checkpoint, E2F targets, mitotic spindle, and epithelial-mesenchymal transition (**Figure 2B**, **2C**). ssGSEA analysis of 369 samples showed a positive correlation of ZNF248 with G2M checkpoint, E2F targets, and mitotic spindle (**Figure 2D**). GO analysis indicated that the most enriched terms in BP were embryonic organ development, synapse organization, and cell-cell adhesion (**Figure 2E**). In terms of CC, enrichment was mainly observed in synaptic membrane, apical part of the cell, and transporter complex (**Figure 2F**). For MF, terms related to channel activity and transmembrane transporter activity were predominantly enriched (**Figure 2G**).

*ZNF248 can reconstruct the immune microenvironment of LIHC*

The immune microenvironment of LIHC samples was evaluated using algorithms like CIBERSORT, MCPcounter, xCell, EPIC, TIMER, QUANTISEQ, and ESTIMATE. The immune infiltration patterns of patients with high and low ZNF248 expression differed (**Figure 3A**). Immunocorrelation showed that ZNF248 increased immune infiltration in the LIHC microenvironment, affecting CD8+ T cells (R = 0.14, P = 0.0089), T cells (R = 0.18, P = 0.00058), B cells (R = 0.38, P = 5.1e-14), fibroblasts (R = 0.29, P = 1.6e-08), endothelial cells (R = 0.28, P = 3.1e-08), macrophages M2 (R = 0.24, P = 2e-06), and Tregs (R = 0.32, P = 3.8e-10), while decreasing NK cell levels (**Figure 3B-I**). An interaction was found between ZNF248 and immunological, estimation, tumor purity, and stromal scores (**Figure 3J-M**). ZNF248 positively correlated with tumor purity score and negatively correlated with immune score. High ZNF248 expression was associated with elevated levels of critical immune checkpoints PDCD1, CD274,

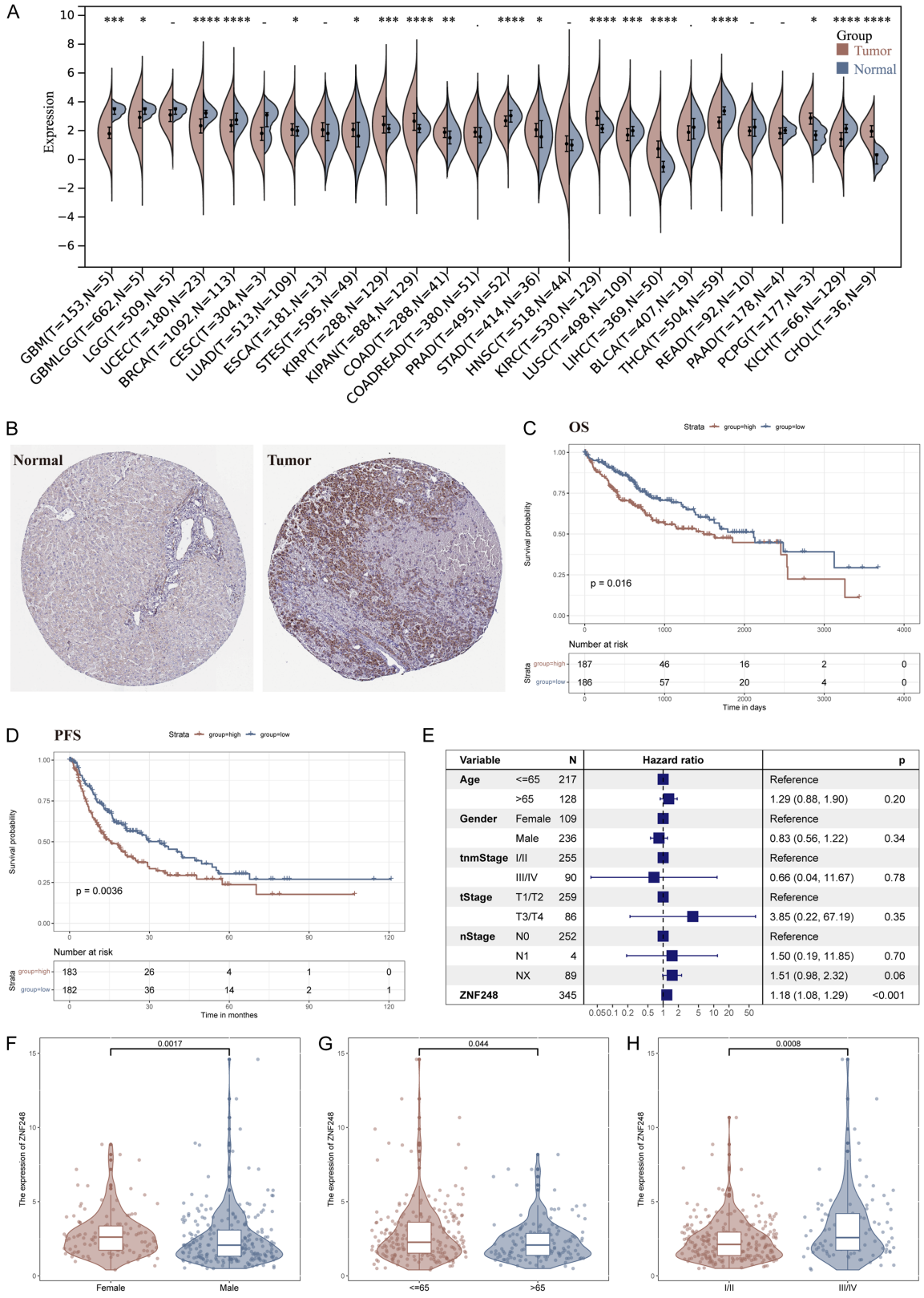


**Figure 1.** Expression pattern and clinical role of ZNF248 in liver cancer. A. The landscape of ZNF248 in pan-cancer. B. Representative immunohistochemical images of ZNF248 from the HPA database. C, D. Prognostic performance of ZNF248 in The Cancer Genome Atlas (TCGA) database. E. Multivariate analysis of ZNF248. F-H. Clinical correlation of ZNF248. *P < 0.05, **P < 0.01, ***P < 0.001.

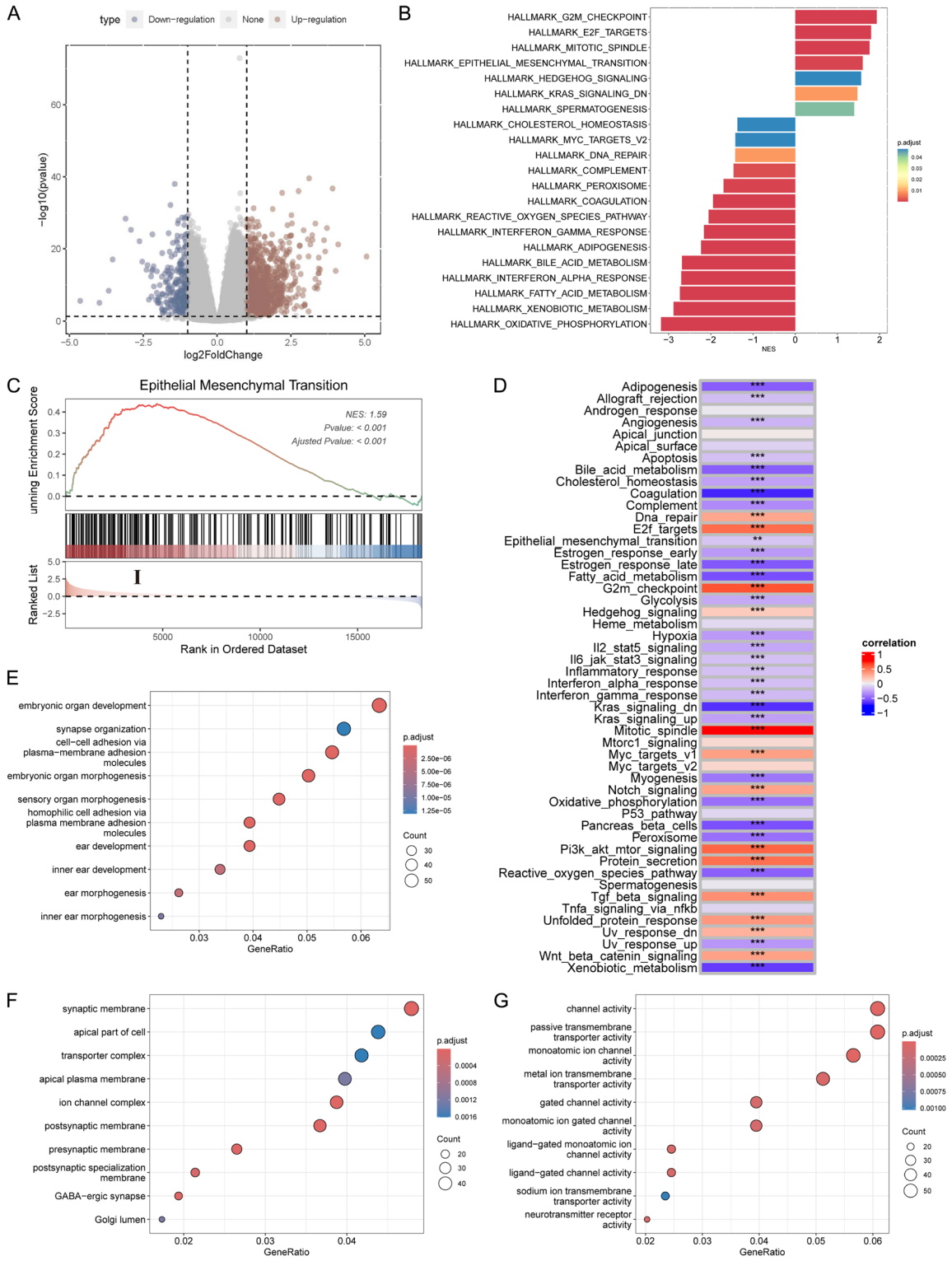


**Figure 2.** The biological role of ZNF248. A. Differentially expressed genes (DEGs) between the high and low ZNF248 expression groups. B, C. Enrichment analysis of the Hallmark gene set using Gene Set Enrichment Analysis (GSEA). D. Correlation between pathways quantified by the Single Sample Gene Set Enrichment Analysis (ssGSEA) algorithm and the expression of ZNF248. E-G. Gene Ontology (GO) analysis of the Differentially Expressed Genes (DEGs). *P < 0.05, **P < 0.01, ***P < 0.001.

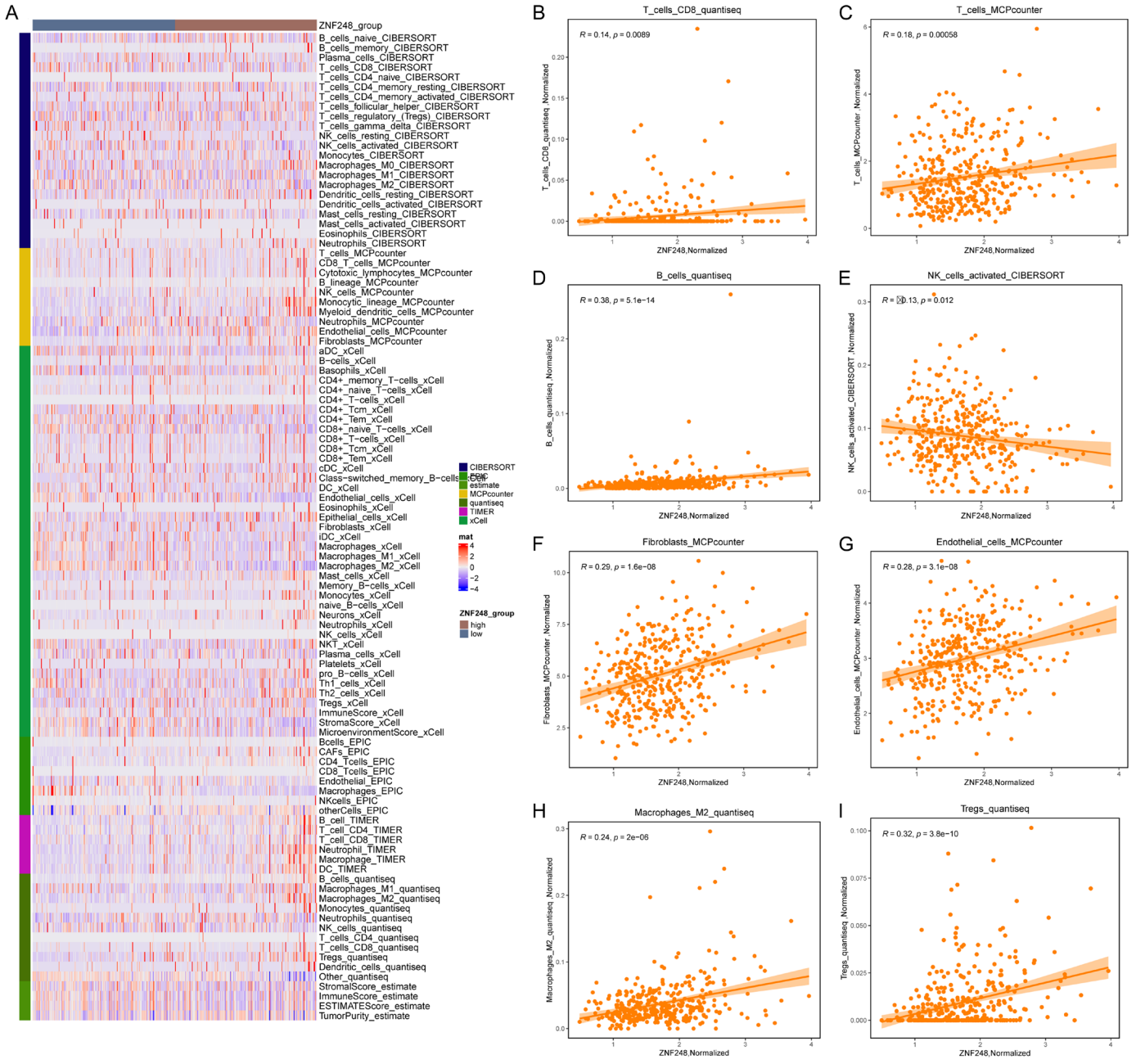
A
ZNF248_group
B_cells_naive_CIBERSORT
B_cells_memory_CIBERSORT
Plasma_cells_CIBERSORT
T_cells_CD8_CIBERSORT
T_cells_CD4_naive_CIBERSORT
T_cells_CD4_memory_resting_CIBERSORT
T_cells_CD4_memory_activated_CIBERSORT
T_cells_follicular_helper_CIBERSORT
T_cells_regulatory_(Tregs)_CIBERSORT
T_cells_gamma_delta_CIBERSORT
NK_cells_resting_CIBERSORT
NK_cells_activated_CIBERSORT
Monocytes_CIBERSORT
Macrophages_M0_CIBERSORT
Macrophages_M1_CIBERSORT
Macrophages_M2_CIBERSORT
Dendritic_cells_resting_CIBERSORT
Dendritic_cells_activated_CIBERSORT
Mast_cells_resting_CIBERSORT
Mast_cells_activated_CIBERSORT
Eosinophils_CIBERSORT
Neutrophils_CIBERSORT
T_cells_MCPcounter
CD8_T_cells_MCPcounter
Cytotoxic_lymphocytes_MCPcounter
B_lineage_MCPcounter
NK_cells_MCPcounter
Monocytic_lineage_MCPcounter
Myeloid_dendritic_cells_MCPcounter
Neutrophils_MCPcounter
Endothelial_cells_MCPcounter
Fibroblasts_MCPcounter
aDC_xCell
B−cells_xCell
Basophils_xCell
CD4+_memory_T−cells_xCell
CD4+_naive_T−cells_xCell
CD4+_T−cells_xCell
CD4+_Tcm_xCell
CD4+_Tem_xCell
CD8+_naive_T−cells_xCell
CD8+_T−cells_xCell
CD8+_Tcm_xCell
CD8+_Tem_xCell
cDC_xCell
Class−switched_memory_B−cells_xCell
DC_xCell
Endothelial_cells_xCell
Eosinophils_xCell
Epithelial_cells_xCell
Fibroblasts_xCell
iDC_xCell
Macrophages_xCell
Macrophages_M1_xCell
Macrophages_M2_xCell
Mast_cells_xCell
Memory_B−cells_xCell
Monocytes_xCell
naive_B−cells_xCell
Neurons_xCell
Neutrophils_xCell
NK_cells_xCell
NKT_xCell
Plasma_cells_xCell
Platelets_xCell
pro_B−cells_xCell
Th1_cells_xCell
Th2_cells_xCell
Tregs_xCell
ImmuneScore_xCell
StromaScore_xCell
MicroenvironmentScore_xCell
Bcells_EPIC
CAFs_EPIC
CD4_Tcells_EPIC
CD8_Tcells_EPIC
Endothelial_EPIC
Macrophages_EPIC
NKcells_EPIC
otherCells_EPIC
B_cell_TIMER
T_cell_CD4_TIMER
T_cell_CD8_TIMER
Neutrophil_TIMER
Macrophage_TIMER
DC_TIMER
B_cells_quantiseq
Macrophages_M1_quantiseq
Macrophages_M2_quantiseq
Monocytes_quantiseq
Neutrophils_quantiseq
NK_cells_quantiseq
T_cells_CD4_quantiseq
T_cells_CD8_quantiseq
Tregs_quantiseq
Dendritic_cells_quantiseq
Other_quantiseq
StromalScore_estimate
ImmuneScore_estimate
ESTIMATEScore_estimate
TumorPurity_estimate
CIBERSORT
cell_type
estimate
MCPcounter
quantiseq
TIMER
xCell
mat
4
2
0
−2
−4
ZNF248_group
high
low
B
T_cells_CD8_quantiseq
R = 0.14, p = 0.0089
T_cells_CD8_quantiseq_Normalized
ZNF248,Normalized
C
T_cells_MCPcounter
R = 0.18, p = 0.00058
T_cells_MCPcounter_Normalized
ZNF248,Normalized
D
B_cells_quantiseq
R = 0.38, p = 5.1e−14
B_cells_quantiseq_Normalized
ZNF248,Normalized
E
NK_cells_activated_CIBERSORT
R = −0.13, p = 0.012
NK_cells_activated_CIBERSORT_Normalized
ZNF248,Normalized
F
Fibroblasts_MCPcounter
R = 0.29, p = 1.6e−08
Fibroblasts_MCPcounter_Normalized
ZNF248,Normalized
G
Endothelial_cells_MCPcounter
R = 0.28, p = 3.1e−08
Endothelial_cells_MCPcounter_Normalized
ZNF248,Normalized
H
Macrophages_M2_quantiseq
R = 0.24, p = 2e−06
Macrophages_M2_quantiseq_Normalized
ZNF248,Normalized
I
Tregs_quantiseq
R = 0.32, p = 3.8e−10
Tregs_quantiseq_Normalized
ZNF248,Normalized

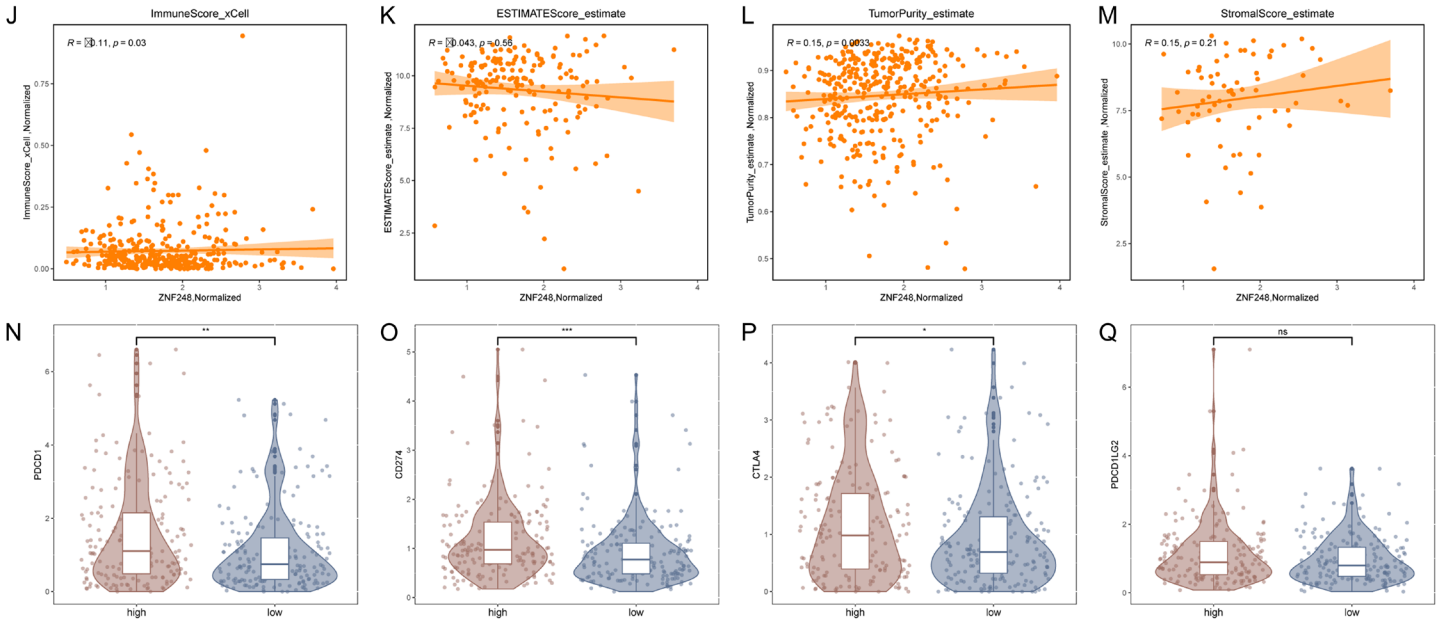


**Figure 3.** The immune landscape of ZNF248 in liver cancer. A. Immune cell infiltration in the Tumor Microenvironment (TME) of liver cancer between high and low ZNF248 expression groups. B-I. Correlation between ZNF248 and multiple immune cells. J-M. Correlation of ZNF248 with immune score, estimate score, tumor purity score, and stromal score. N-Q. The expression levels of immune escape genes between high and low ZNF248 expression groups.

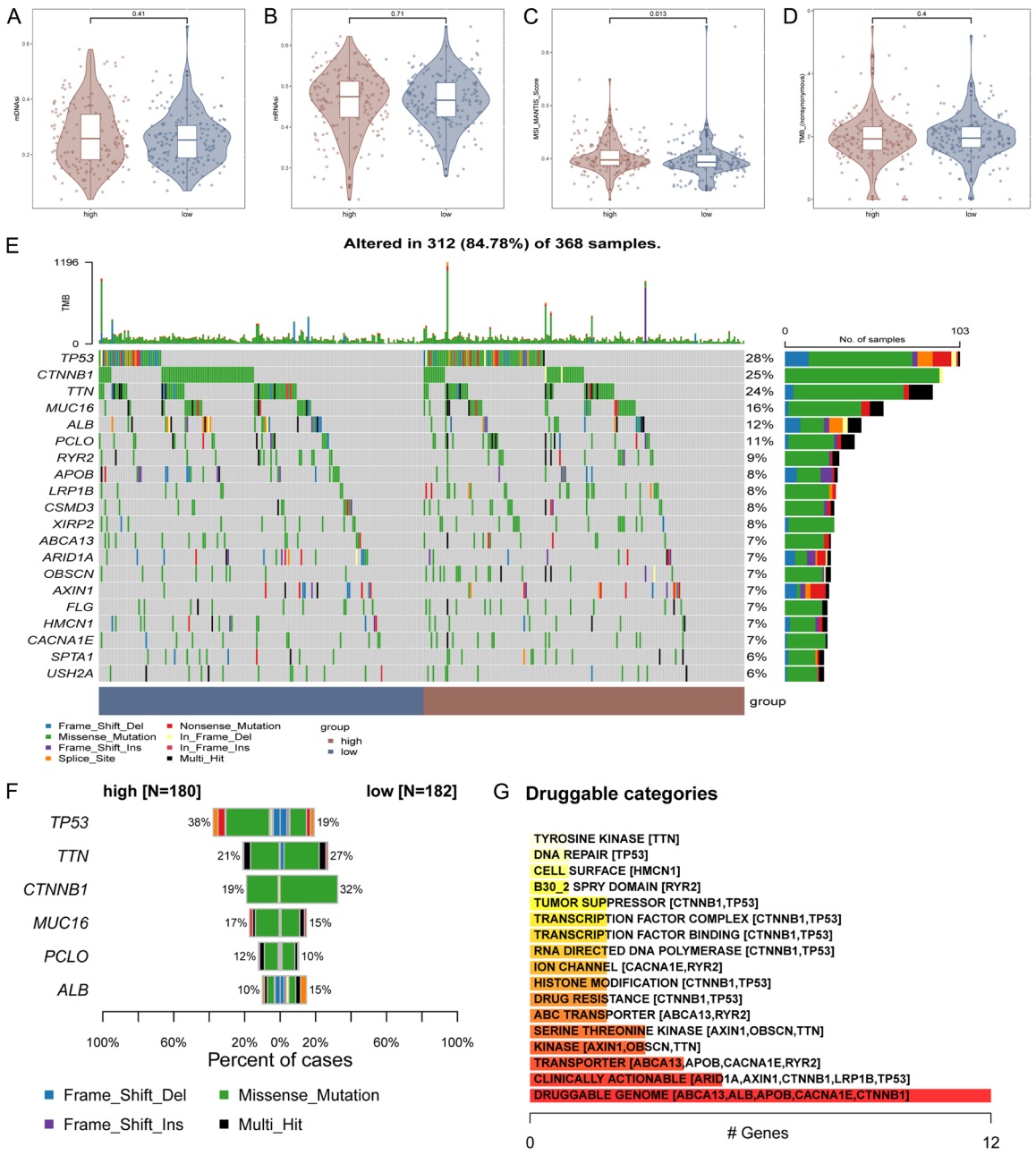


**Figure 4.** Genomic characteristics of ZNF248. A-D. Correlation of ZNF248 with mDNAsi, mRNAsi, Microsatellite Instability (MSI), and Tumor Mutation Burden (TMB). E, F. Mutation characteristics of high and low ZNF248 expression groups. G. Drug-gene interactions and gene druggability information.

and CTLA4, indicating a potential impact on the immunotherapeutic response and the effectiveness of immune checkpoint inhibitors in LIHC patients (**Figure 3N-Q**).

*Role of ZNF248 in genomic characterization of LIHC*

MSI is a crucial marker for cancer immunotherapy [33]. We examined the relationship between ZNF248 and MSI, TMB, mRNAsi, and mDNAsi (**Figure 4A-D**). The findings demonstrated a favorable correlation between ZNF248 and MSI (**Figure 4C**). In patients with high and low ZNF248 expression, the top 3 genes with the most differential mutations were TP53, CTNNB1, and TTN (**Figure 4E**). The highest percentage of differentially mutated genes was TP53 in the high-expression group, with missense mutation being the most frequent muta-

tion type in both high and low ZNF248 expression groups (**Figure 4F**). Drug-gene interactions and potential drug targets revealed 12 genes as potential drug targets, mainly associated with clinically actionable transporter and kinase (**Figure 4G**).

*Immunotherapy response, drug sensitivity, and nomogram mapping of ZNF248 in LIHC patients*

The TIDE score for each LIHC patient was calculated. ZNF248 was positively correlated with TIDE score and immune rejection and negatively correlated with immune dysfunction (**Figure 5A-C**). Further analysis indicated a correlation between high ZNF248 expression and non-responders to immunotherapy (**Figure 5D**). ZNF248 showed a negative correlation with ips_CTLA4_neg_PD1_neg, suggesting its influence on immune therapy response (**Figure 5E**). ZNF248 promoted the sensitivity to Cabozantinib while decreasing sensitivity to Dacomitinib and Pentostatin (**Figure 5F-H**). A nomogram plot incorporating ZNF248 expression and clinical characteristics was created (**Figure 5I**). Calibration curves showed good agreement between actual and predicted survival (**Figure 5J**).

*Co-expression analysis of ZNF248-related genes based on WGCNA*

WGCNA clustering analysis identified the optimal soft threshold as 12 (**Figure 5K**). A gene clustering tree was constructed, dividing genes into 9 modules, with the turquoise module exhibiting the highest correlation with ZNF248 (R = 0.77, P = 3e-75) (**Figure 5L**).

*Machine learning identified prognostic signature based on ZNF248-derived molecules*

LASSO logistic regression identified 10 relevant hub genes among 221 genes (**Figure 6A**). Multivariable Cox regression analysis determined prognostic signatures, revealing a positive correlation between BMI1 and prognosis (OR = 1.03, 95% CI = 1.00 to 1.05, P = 0.02) (**Figure 6B**). Data from 259 TCGA patients were used as a training set, and 115 LIHC patients were used for external validation. Patients in the lower-risk group had better OS in both cohorts, indicating that low expression predicted a better prognosis (**Figure 6C**, **6D**). The prognostic model demonstrated good predictive ability for patient survival (**Figure 6E**, 1-year AUC = 0.79; 3-year AUC = 0.76; 5-year AUC = 0.74; **Figure 6F**, 1-year AUC = 0.66; 3-year AUC = 0.72; 5-year AUC = 0.80). A positive correlation was observed between the risk score and TIDE score, as well as immune exclusion (**Figure 6G**, TIDE, R = 0.51, P = 6e-09; **Figure 6I**, Exclusion, R = 0.54, P = 6.1e-10), while a negative correlation was found with immune dysfunction (**Figure 6H**, R = -0.67, P = 4.2e-16). Non-responders to immunotherapy tended to have higher risk scores (**Figure 6J**).

*ZNF248 promotes aggressive traits in HCC cells*

RT-qPCR results revealed significant overexpression of ZNF248 in HCC cells compared to control cells (**Figure 7A**). The efficiency of ZNF248 knockdown and overexpression is shown in **Figure 7B**. CCK8 assays demonstrated that silencing ZNF248 significantly reduced Huh-7 cell proliferation, while overexpressing ZNF248 increased MHCC97H cell proliferation (**Figure 7C** and **7D**). These findings were corroborated by colony formation assays (**Figure 7E** and **7F**). EdU incorporation decreased in ZNF248-silenced Huh-7 cells and increased in ZNF248-overexpressing MHCC97H cells (**Figure 7G** and **7H**). Transwell migration and invasion assays showed that ZNF248 knockdown markedly reduced Huh-7 cell migratory and invasive abilities, while ZNF248 overexpression enhanced these capabilities in MHCC97H cells (**Figure 7I** and **7J**). These results underscore ZNF248's role in promoting invasion and progression of HCC cells.

*ZNF248 promotes HCC proliferation and invasion via the PI3K-AKT signaling pathway*

To investigate the mechanism by which ZNF248 regulates HCC proliferation and invasion, Gene Set Enrichment Analysis (GSEA) was performed. The results indicated that the related genes were enriched in the PI3K-AKT signaling pathway (**Figure 8A**). Western blot analysis revealed that the PI3K-AKT signaling pathway was inhibited when ZNF248 was silenced by siRNA, and this inhibition was reversed by the PI3K-AKT signaling pathway agonist SC79 (**Figure 8B**). Functional assays, including CCK8, EdU, Transwell, and colony formation assays, demonstrated that silencing ZNF248 inhibited the prolifer-

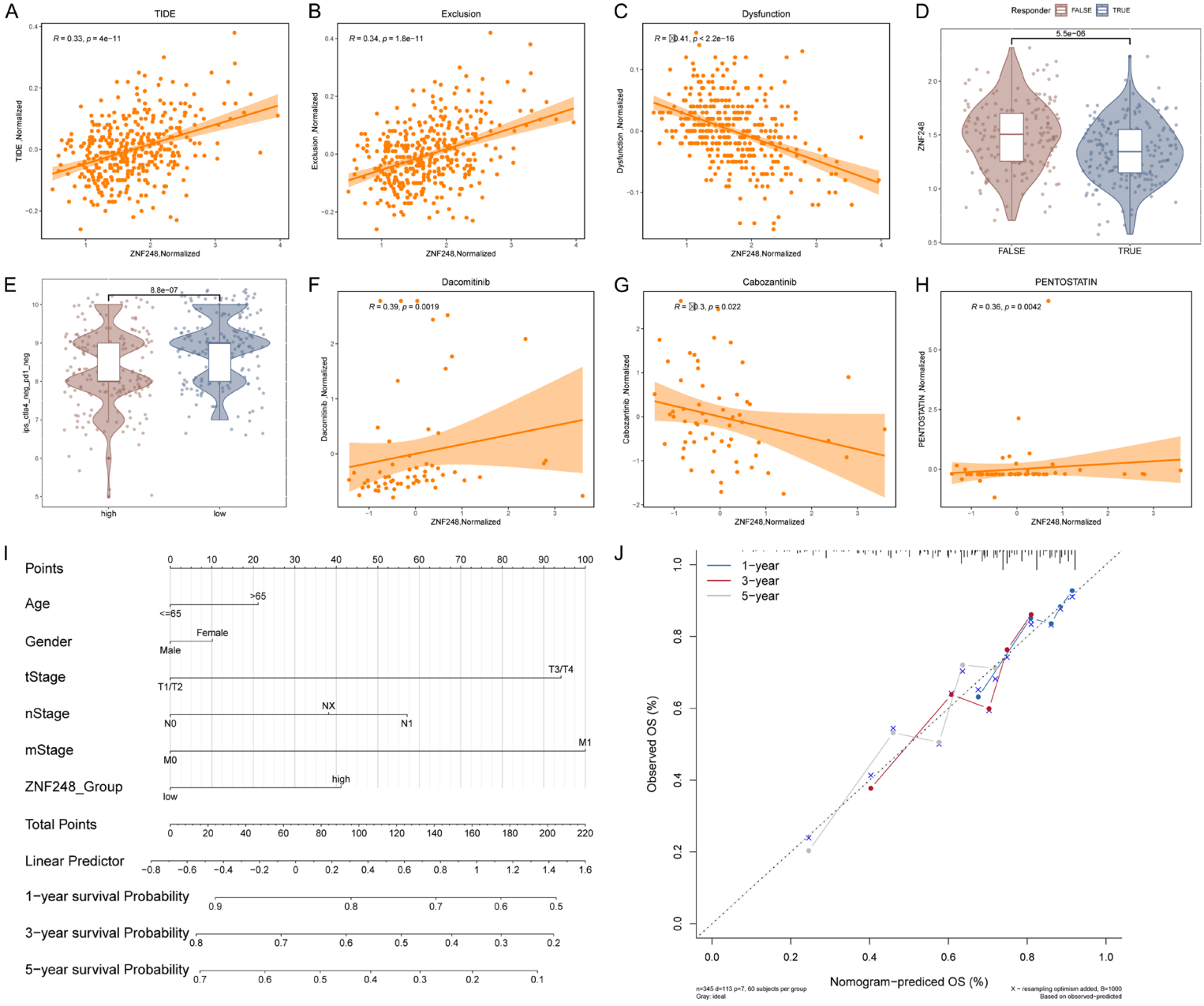
A
TIDE
R = 0.33, p = 4e−11
TIDE_Normalized
ZNF248_Normalized
B
Exclusion
R = 0.34, p = 1.8e−11
Exclusion_Normalized
ZNF248_Normalized
C
Dysfunction
R = −0.41, p < 2.2e−16
Dysfunction_Normalized
ZNF248_Normalized
D
Responder FALSE TRUE
5.5e−06
ZNF248
FALSE
TRUE
E
8.8e−07
ips_ctla4_neg_pd1_neg
high
low
F
Dacomitinib
R = 0.39, p = 0.0019
Dacomitinib_Normalized
ZNF248_Normalized
G
Cabozantinib
R = −0.3, p = 0.022
Cabozantinib_Normalized
ZNF248_Normalized
H
PENTOSTATIN
R = 0.36, p = 0.0042
PENTOSTATIN_Normalized
ZNF248_Normalized
I
Points
Age
>65
<=65
Gender
Female
Male
tStage
T3/T4
T1/T2
nStage
NX
N0
N1
mStage
M1
M0
ZNF248_Group
high
low
Total Points
Linear Predictor
1−year survival Probability
3−year survival Probability
5−year survival Probability
J
1−year
3−year
5−year
Observed OS (%)
Nomogram−prediced OS (%)
n=345 d=113 p=7, 60 subjects per group
Gray: ideal
X − resampling optimism added, B=1000
Based on observed−predicted

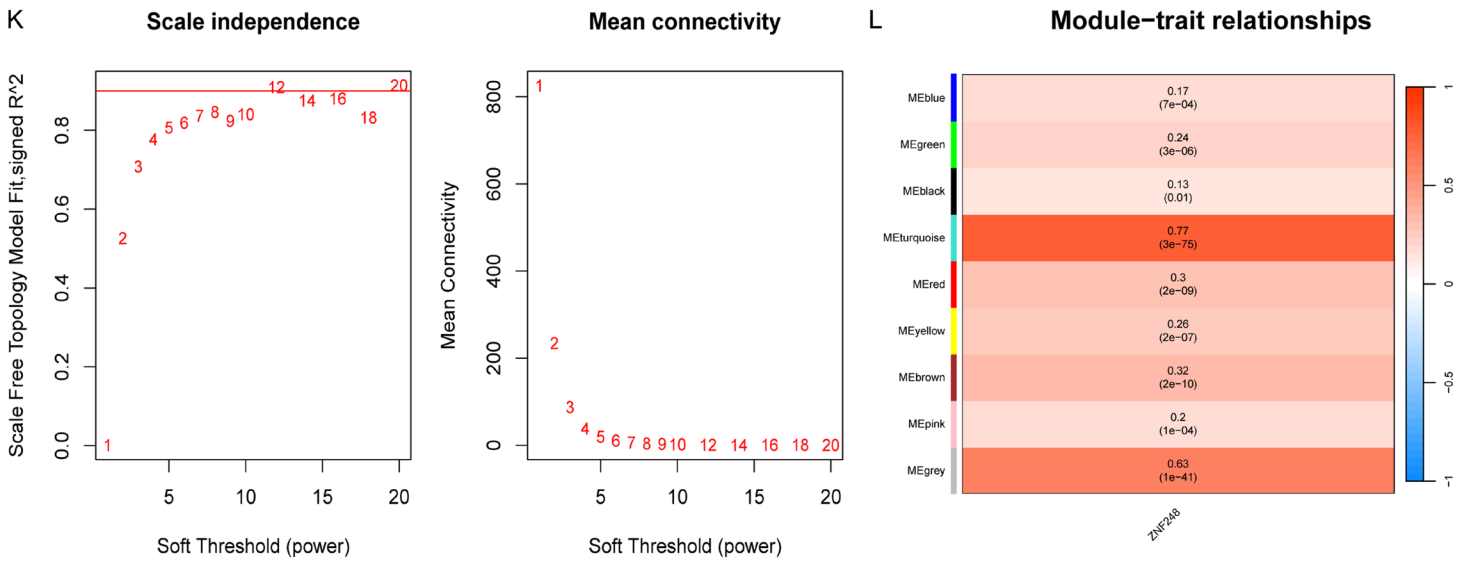


**Figure 5.** The intersection of ZNF248 with immunotherapy and drug sensitivity. A-C. Correlation of ZNF248 with Tumor Immune Dysfunction and Exclusion (TIDE) score, immune exclusion score, and immune dysfunction score. D. Analyzing ZNF248 expression in responders and non-responders to immunotherapy. E. The Immunophenoscore (IPS) score in high and low ZNF248 expression groups. F-H. Correlation of ZNF248 with drug sensitivity. I. The nomogram plot based on ZNF248. J. The calibration curve for 1, 3, and 5 years. K. Optimal power value of Weighted Gene Co-expression Network Analysis (WGCNA). L. Correlation analysis between gene modules and ZNF248.

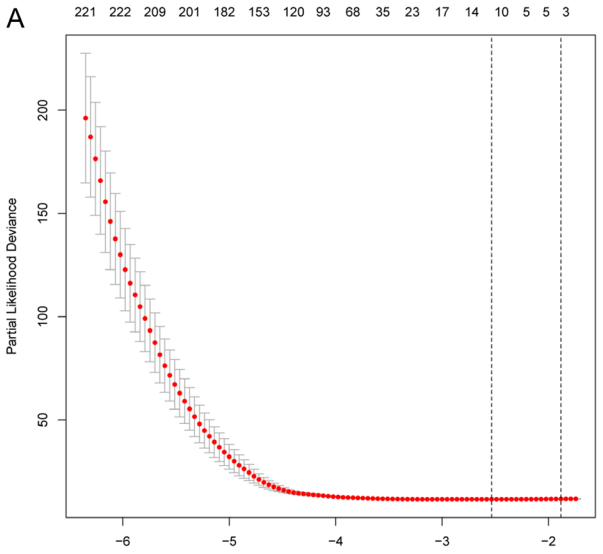


B

| Variable | N | Hazard ratio | p |
|---|---|---|---|
| YBX1 | 259 | 1.00 (1.00, 1.00) | 0.12 |
| SF3B4 | 259 | 1.00 (1.00, 1.00) | 0.60 |
| TIMM23 | 259 | 1.01 (1.00, 1.01) | 0.17 |
| PPM1G | 259 | 1.00 (0.99, 1.01) | 0.86 |
| RTN3 | 259 | 1.00 (0.99, 1.01) | 0.71 |
| ATIC | 259 | 1.00 (1.00, 1.01) | 0.38 |
| SEPHS1 | 259 | 0.99 (0.98, 1.01) | 0.55 |
| MED8 | 259 | 1.00 (0.99, 1.02) | 0.63 |
| BMI1 | 259 | 1.03 (1.00, 1.05) | 0.02 |
| CDCA8 | 259 | 1.01 (0.99, 1.03) | 0.62 |



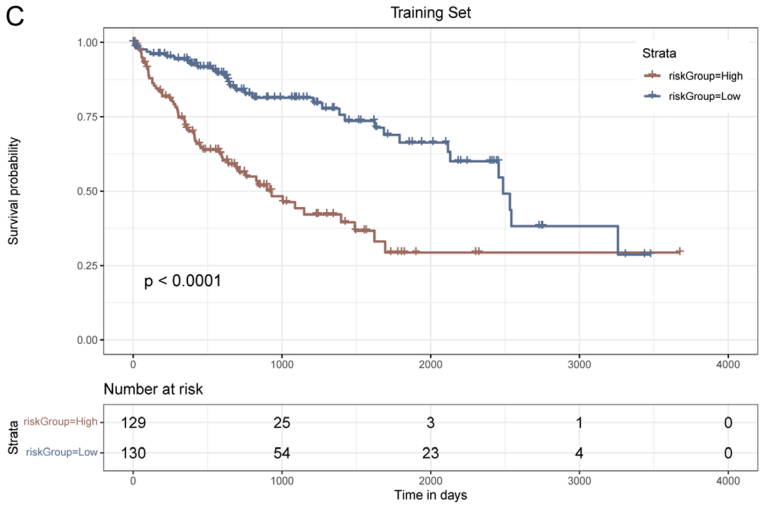


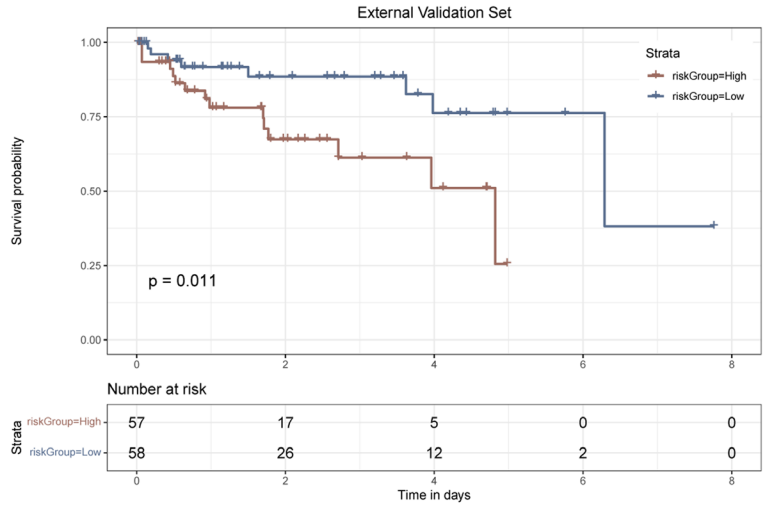

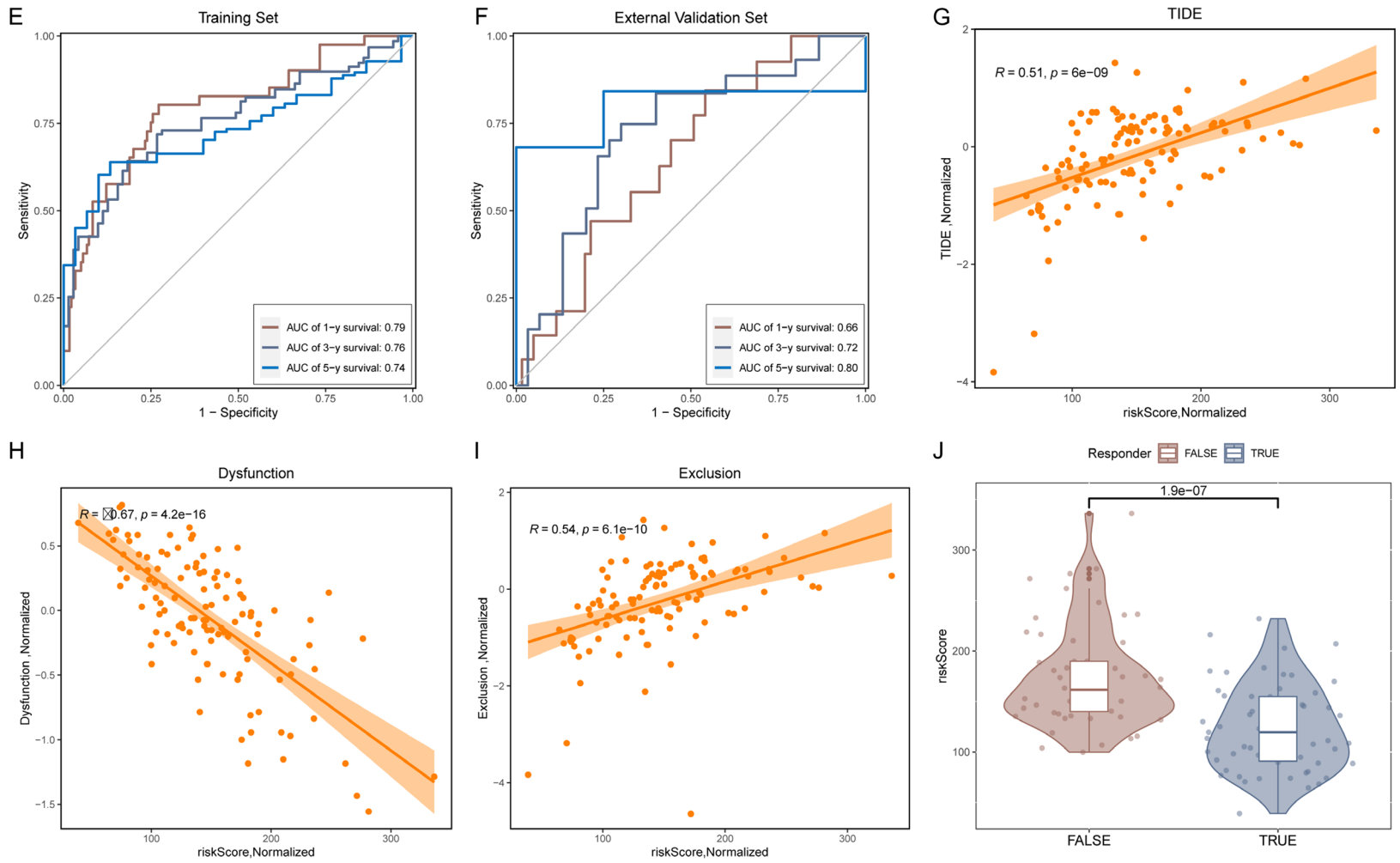


**Figure 6.** Identification of the prognostic signature from ZNF248-related genes. A. Least Absolute Shrinkage and Selection Operator (LASSO) regression was utilized to identify the hub genes. B. Multivariate Cox regression analysis on genes included in the signature. C-F. The performance of the signature in predicting patient survival in the training and external validation sets. G-I. Correlation of risk score with Tumor Immune Dysfunction and Exclusion (TIDE) score, immune exclusion score, and immune dysfunction score. J. Analyzing risk score in responders and non-responders to immunotherapy.

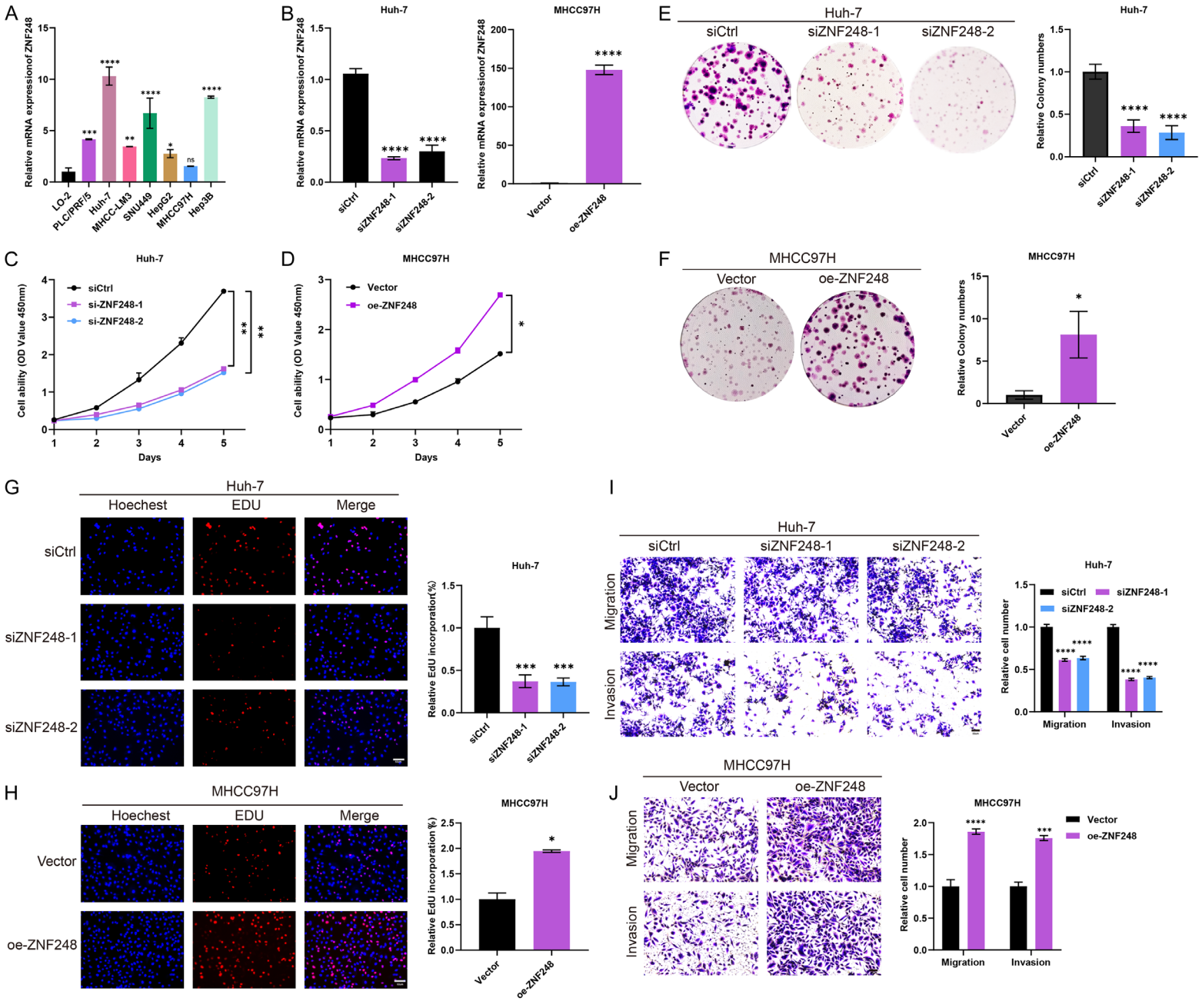
A
Relative mRNA expressionof ZNF248
LO-2
PLC/PRF/5
Huh-7
MHCC-LM3
SNU449
HepG2
MHCC97H
Hep3B
B
Huh-7
Relative mRNA expressionof ZNF248
siCtrl
siZNF248-1
siZNF248-2
MHCC97H
Vector
oe-ZNF248
E
Huh-7
siCtrl
siZNF248-1
siZNF248-2
Relative Colony numbers
C
Huh-7
siCtrl
si-ZNF248-1
si-ZNF248-2
Cell ability (OD Value 450nm)
Days
D
MHCC97H
Vector
oe-ZNF248
F
MHCC97H
Vector
oe-ZNF248
Relative Colony numbers
G
Huh-7
Hoechest
EDU
Merge
siCtrl
siZNF248-1
siZNF248-2
Relative EdU incorporation(%)
H
MHCC97H
Vector
oe-ZNF248
I
Huh-7
Migration
Invasion
Relative cell number
J
MHCC97H

**Figure 7.** ZNF248 promotes the malignant biological behaviors of HCC cells. (A) ZNF248 mRNA expression levels detected by Reverse Transcription Quantitative Polymerase Chain Reaction (RT-qPCR). (B) Knockdown and overexpression efficiency of ZNF248 siRNA and pcDNA detected by RT-qPCR. Functional assays were conducted to assess ZNF248 regulation of Hepatocellular Carcinoma (HCC) cell proliferation and invasion, including: (C, D) Cell Counting Kit-8 (CCK-8) assays, (E, F) Colony formation assays, (G, H) 5-Ethynyl-2'-deoxyuridine (EdU) assays, (I, J) Transwell assays. *P < 0.05, **P < 0.01, ***P < 0.001, ****P < 0.0001.

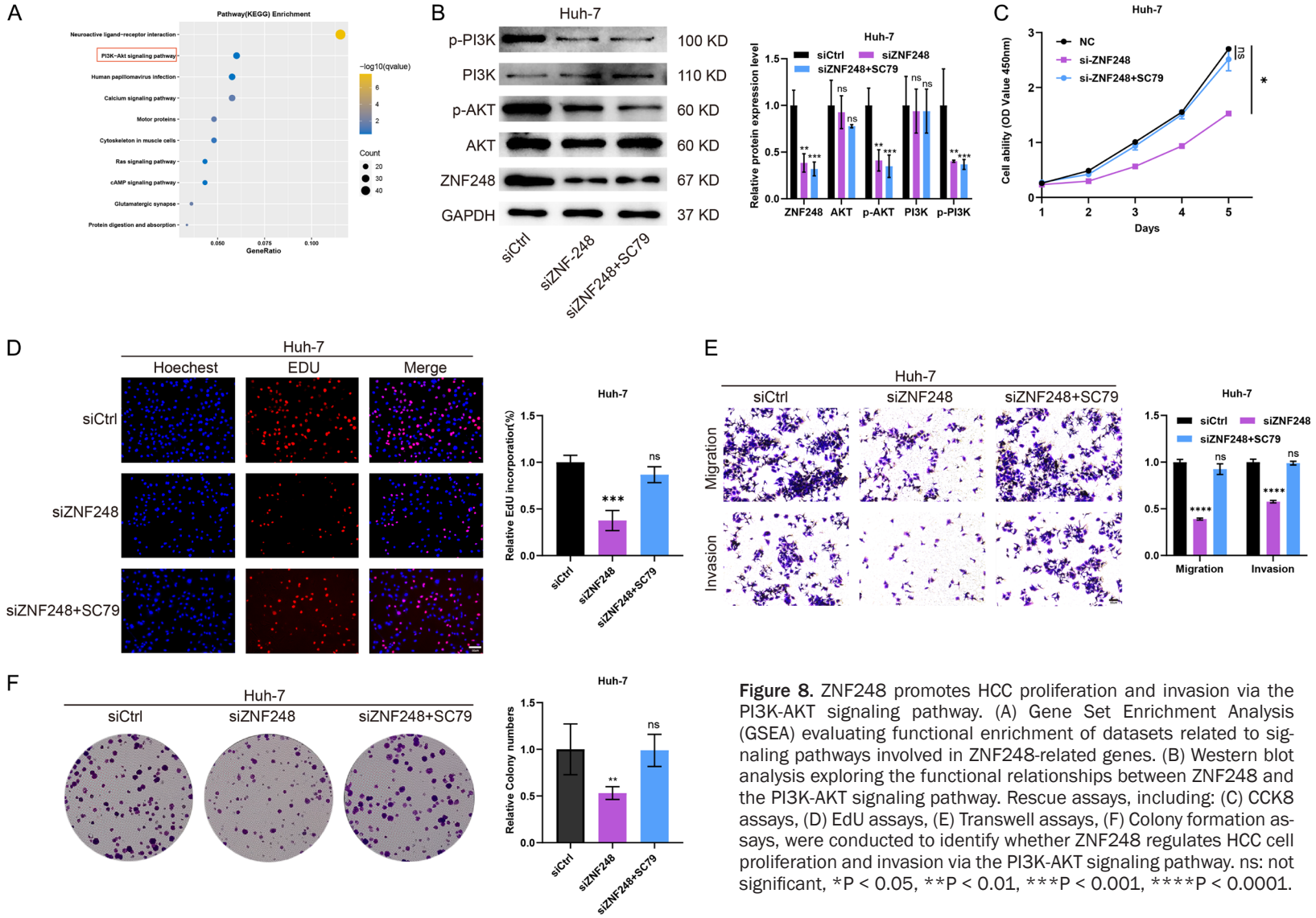


**Figure 8.** ZNF248 promotes HCC proliferation and invasion via the PI3K-AKT signaling pathway. (A) Gene Set Enrichment Analysis (GSEA) evaluating functional enrichment of datasets related to signaling pathways involved in ZNF248-related genes. (B) Western blot analysis exploring the functional relationships between ZNF248 and the PI3K-AKT signaling pathway. Rescue assays, including: (C) CCK8 assays, (D) EdU assays, (E) Transwell assays, (F) Colony formation assays, were conducted to identify whether ZNF248 regulates HCC cell proliferation and invasion via the PI3K-AKT signaling pathway. ns: not significant, *P < 0.05, **P < 0.01, ***P < 0.001, ****P < 0.0001.

ation and invasion of HCC cells, and these effects were reversed by SC79 (**Figure 8C-F**).

## Discussion

Liver hepatocellular carcinoma (LIHC) is one of the most prevalent malignancies globally, characterized by high incidence and mortality rates. The World Health Organization predicts that over 1 million individuals could succumb to liver cancer by 2030 [1, 34]. LIHC is often diagnosed at an advanced stage due to the low rate of early detection and its rapid progression, which significantly limits treatment options. Therefore, identifying new biomarkers as prognostic and therapeutic targets is essential for improving LIHC patient outcomes.

In this study, we utilized multiple bioinformatics approaches to demonstrate that higher ZNF248 expression in LIHC is associated with adverse clinicopathologic features, shorter survival time, and a poorer prognosis. Our results indicate that ZNF248 is significantly upregulated in LIHC patients, as confirmed by immunohistochemistry. High ZNF248 expression was correlated with worse overall survival (OS) and progression-free survival (PFS). Furthermore, COX regression analysis identified ZNF248 as an independent risk factor for LIHC, with significantly higher expression in patients at TNM Stage III/IV. These findings were validated by functional experiments, confirming that ZNF248 promotes LIHC progression.

To further elucidate the molecular mechanisms underlying ZNF248's role in LIHC, we conducted bioenrichment analysis to identify pathways in which ZNF248 is involved. Gene Set Enrichment Analysis (GSEA) and single-sample GSEA (ssGSEA) of the Hallmark gene set indicated that ZNF248 is primarily enriched in processes related to the G2/M checkpoint, E2F targets, mitotic spindle, and epithelial-mesenchymal transition (EMT). The G2/M checkpoint is crucial for regulating cell entry into mitosis, thereby preventing abnormal proliferation and allowing genomic surveillance and DNA repair [35]. For example, apigetrin-induced cell cycle arrest at the G2/M phase has been shown to suppress proliferation in Hep3B cells [36]. E2Fs, which are potential therapeutic targets for LIHC, play critical roles in cell proliferation, apoptosis, differentiation, senescence, and the DNA damage response [37]. Our findings suggest a positive correlation between ZNF248 and these cell cycle-related regulators, implying that ZNF248 may influence pivotal checkpoints in the LIHC cell cycle.

The tumor immune microenvironment (TME) is a key determinant of tumor growth, proliferation, and therapeutic response [38]. In our analysis, different ZNF248 expression levels in LIHC samples were associated with distinct immune infiltration patterns. Specifically, high ZNF248 expression correlated with increased infiltration of CD8+ T cells, T cells, B cells, fibroblasts, endothelial cells, M2 macrophages, and regulatory T cells (Tregs). These immune components play crucial roles in cancer development and immune evasion. For example, IFNγ(-) IL-17(+) CD8 T cells contribute to immunosuppression and tumor progression in LIHC, and their presence is associated with poor prognosis [39]. Similarly, tumor-infiltrating B cells, despite their relatively low abundance, have been found to correlate with poor differentiation and promote hepatocarcinogenesis [40]. Furthermore, exosomes derived from highly metastatic cancer cells can activate fibroblasts, promoting LIHC lung metastasis [41]. Tregs, both circulating and within tumors, contribute to LIHC progression by impairing the effector function of CD8+ T cells, particularly in hepatitis B virus (HBV)-related cases [42]. Our results indicate that ZNF248 may function as an immune-associated molecule, with potential implications for remodeling the TME in LIHC patients.

Tumor immunotherapy, which aims to overcome immune escape mechanisms and reactivate immune cells to eliminate cancer cells, has emerged as a promising treatment strategy for LIHC [43]. In our study, we observed higher expression of immune checkpoint genes in the ZNF248_high group. Additionally, higher Tumor Immune Dysfunction and Exclusion (TIDE) scores were noted in this group, suggesting reduced efficacy of immune checkpoint inhibition and a higher probability of immune escape in patients with elevated ZNF248 expression [23]. This highlights the potential role of ZNF248 in modulating the response to immunotherapy in LIHC.

To assess the prognostic value of ZNF248, we developed a prognostic signature based on ZNF248-related molecules using the Least

Absolute Shrinkage and Selection Operator (LASSO) algorithm on TCGA data, and validated it with the GSE76427 dataset. The prognostic signature demonstrated good predictive performance for patient survival, underscoring the biological significance of ZNF248 in LIHC. However, the study has several limitations. Most of the data were derived from the TCGA database, which may limit the generalizability of our findings to different populations. Future research should aim to validate our results using local clinical data to ensure broader applicability. Additionally, although we explored the biological features and functions of ZNF248 in LIHC, its specific mechanistic role requires further investigation through detailed molecular studies.

## Conclusion

In summary, our study identifies ZNF248 as a novel immunotherapeutic biomarker that influences the immune microenvironment in LIHC. ZNF248 has a broad regulatory role, including the modulation of the TME, impacting immunotherapeutic response and prognostic assessment. This study is the first to report on the biological role of ZNF248 in LIHC, advancing our understanding of its potential in targeted prevention, treatment, monitoring, and prognostic evaluation of this malignancy.

## Disclosure of conflict of interest

None.

**Address correspondence to:** Feng Jin, Department of Gastroenterology, Cangshan Hospital, The 900Th Hospital of Joint Logistics Support Force of Chinese People's Liberation Army, No. 90, guocuoli, Jianxin Town, Cangshan District, Fuzhou, Fujian, The People's Republic of China. Tel: +86-13706962286; E-mail: JinfAndy@163.com

## References

[1] Sung H, Ferlay J, Siegel RL, Laversanne M, Soerjomataram I, Jemal A and Bray F. Global cancer statistics 2020: GLOBOCAN estimates of incidence and mortality worldwide for 36 cancers in 185 countries. CA Cancer J Clin 2021; 71: 209-249.

[2] Donne R and Lujambio A. The liver cancer immune microenvironment: therapeutic implications for hepatocellular carcinoma. Hepatology 2023; 77: 1773-1796.

[3] Forner A, Reig M and Bruix J. Hepatocellular carcinoma. Lancet 2018; 391: 1301-1314.

[4] Liu CY, Chen KF and Chen PJ. Treatment of liver cancer. Cold Spring Harb Perspect Med 2015; 5: a021535.

[5] Guy J, Hearn T, Crosier M, Mudge J, Viggiano L, Koczan D, Thiesen HJ, Bailey JA, Horvath JE, Eichler EE, Earthrowl ME, Deloukas P, French L, Rogers J, Bentley D and Jackson MS. Genomic sequence and transcriptional profile of the boundary between pericentromeric satellites and genes on human chromosome arm 10p. Genome Res 2003; 13: 159-172.

[6] Zuo Z. Quantifying the arms race between LINE-1 and KRAB-zinc finger genes through TECookbook. NAR Genom Bioinform 2023; 5: lqad078.

[7] Shukla R, Upton KR, Muñoz-Lopez M, Gerhardt DJ, Fisher ME, Nguyen T, Brennan PM, Baillie JK, Collino A, Ghisletti S, Sinha S, Iannelli F, Radaelli E, Dos Santos A, Rapoud D, Guettier C, Samuel D, Natoli G, Carninci P, Ciccarelli FD, Garcia-Perez JL, Faivre J and Faulkner GJ. Endogenous retrotransposition activates oncogenic pathways in hepatocellular carcinoma. Cell 2013; 153: 101-111.

[8] Yuan P, Wang S, Du T, Liu L, Chen X, Yan J, Han S, Peng B, He X and Liu W. ZNF219, a novel transcriptional repressor, inhibits transcription of the prototype foamy virus by interacting with the viral LTR promoter. Virus Res 2023; 334: 199161.

[9] He L, Fan X, Li Y, Chen M, Cui B, Chen G, Dai Y, Zhou D, Hu X and Lin H. Overexpression of zinc finger protein 384 (ZNF 384), a poor prognostic predictor, promotes cell growth by upregulating the expression of Cyclin D1 in hepatocellular carcinoma. Cell Death Dis 2019; 10: 444.

[10] Xie W, Qiao X, Shang L, Dou J, Yang X, Qiao S and Wu Y. Knockdown of ZNF233 suppresses hepatocellular carcinoma cell proliferation and tumorigenesis. Gene 2018; 679: 179-185.

[11] Wang Y, Gong Y, Li X, Long W, Zhang J, Wu J and Dong Y. Targeting the ZNF-148/miR-335/SOD2 signaling cascade triggers oxidative stress-mediated pyroptosis and suppresses breast cancer progression. Cancer Med 2023; 12: 21308-21320.

[12] Zhao X, Yue Y, Wang X and Zhang Q. Bioinformatics analysis of PLA2G7 as an immune-related biomarker in COPD by promoting expansion and suppressive functions of MDSCs. Int Immunopharmacol 2023; 120: 110399.

[13] Subramanian A, Tamayo P, Mootha VK, Mukherjee S, Ebert BL, Gillette MA, Paulovich A, Pomeroy SL, Golub TR, Lander ES and Mesirov JP. Gene set enrichment analysis: a knowledge-based approach for interpreting

genome-wide expression profiles. Proc Natl Acad Sci U S A 2005; 102: 15545-15550.
[14] Chen Y, Feng Y, Yan F, Zhao Y, Zhao H and Guo Y. A novel immune-related gene signature to identify the tumor microenvironment and prognose disease among patients with oral squamous cell carcinoma patients using ssGSEA: a bioinformatics and biological validation study. Front Immunol 2022; 13: 922195.
[15] Yu G, Wang LG, Han Y and He QY. clusterProfiler: an R package for comparing biological themes among gene clusters. OMICS 2012; 16: 284-287.
[16] The Gene Ontology Consortium. The gene ontology resource: 20 years and still GOing strong. Nucleic Acids Res 2019; 47: D330-D338.
[17] Chen B, Khodadoust MS, Liu CL, Newman AM and Alizadeh AA. Profiling tumor infiltrating immune cells with CIBERSORT. Methods Mol Biol 2018; 1711: 243-259.
[18] Lu H, Wu J, Liang L, Wang X and Cai H. Identifying a novel defined pyroptosis-associated long noncoding RNA signature contributes to predicting prognosis and tumor microenvironment of bladder cancer. Front Immunol 2022; 13: 803355.
[19] Aran D, Hu Z and Butte AJ. xCell: digitally portraying the tissue cellular heterogeneity landscape. Genome Biol 2017; 18: 220.
[20] Racle J and Gfeller D. EPIC: a tool to estimate the proportions of different cell types from bulk gene expression data. Methods Mol Biol 2020; 2120: 233-248.
[21] Li T, Fan J, Wang B, Traugh N, Chen Q, Liu JS, Li B and Liu XS. TIMER: a web server for comprehensive analysis of tumor-infiltrating immune cells. Cancer Res 2017; 77: e108-e110.
[22] Finotello F, Mayer C, Plattner C, Laschober G, Rieder D, Hackl H, Krogsdam A, Loncova Z, Posch W, Wilflingseder D, Sopper S, Ijsselsteijn M, Brouwer TP, Johnson D, Xu Y, Wang Y, Sanders ME, Estrada MV, Ericsson-Gonzalez P, Charoentong P, Balko J, de Miranda NFDCC and Trajanoski Z. Molecular and pharmacological modulators of the tumor immune contexture revealed by deconvolution of RNA-seq data. Genome Med 2019; 11: 34.
[23] Wang T, Dai L, Shen S, Yang Y, Yang M, Yang X, Qiu Y and Wang W. Comprehensive molecular analyses of a macrophage-related gene signature with regard to prognosis, immune features, and biomarkers for immunotherapy in hepatocellular carcinoma based on WGCNA and the LASSO algorithm. Front Immunol 2022; 13: 843408.
[24] Charoentong P, Finotello F, Angelova M, Mayer C, Efremova M, Rieder D, Hackl H and Trajanoski Z. Pan-cancer Immunogenomic analyses reveal genotype-immunophenotype relationships and predictors of response to checkpoint blockade. Cell Rep 2017; 18: 248-262.
[25] Malta TM, Sokolov A, Gentles AJ, Burzykowski T, Poisson L, Weinstein JN, Kamińska B, Huelsken J, Omberg L, Gevaert O, Colaprico A, Czerwińska P, Mazurek S, Mishra L, Heyn H, Krasnitz A, Godwin AK, Lazar AJ, Cancer Genome Atlas Research Network; Stuart JM, Hoadley KA, Laird PW, Noushmehr H and Wiznerowicz M. Machine learning identifies stemness features associated with oncogenic dedifferentiation. Cell 2018; 173: 338-354, e315.
[26] Palmeri M, Mehnert J, Silk AW, Jabbour SK, Ganesan S, Popli P, Riedlinger G, Stephenson R, de Meritens AB, Leiser A, Mayer T, Chan N, Spencer K, Girda E, Malhotra J, Chan T, Subbiah V and Groisberg R. Real-world application of tumor mutational burden-high (TMB-high) and microsatellite instability (MSI) confirms their utility as immunotherapy biomarkers. ESMO Open 2022; 7: 100336.
[27] Reinhold WC, Sunshine M, Liu H, Varma S, Kohn KW, Morris J, Doroshow J and Pommier Y. CellMiner: a web-based suite of genomic and pharmacologic tools to explore transcript and drug patterns in the NCI-60 cell line set. Cancer Res 2012; 72: 3499-3511.
[28] Balachandran VP, Gonen M, Smith JJ and DeMatteo RP. Nomograms in oncology: more than meets the eye. Lancet Oncol 2015; 16: e173-180.
[29] Langfelder P and Horvath S. WGCNA: an R package for weighted correlation network analysis. BMC Bioinformatics 2008; 9: 559.
[30] Kang J, Choi YJ, Kim IK, Lee HS, Kim H, Baik SH, Kim NK and Lee KY. LASSO-based machine learning algorithm for prediction of lymph node metastasis in T1 colorectal cancer. Cancer Res Treat 2021; 53: 773-783.
[31] Hajian-Tilaki K. Receiver operating characteristic (ROC) curve analysis for medical diagnostic test evaluation. Caspian J Intern Med 2013; 4: 627-635.
[32] Livak KJ and Schmittgen TD. Analysis of relative gene expression data using real-time quantitative PCR and the 2(-Delta Delta C(T)) method. Methods 2001; 25: 402-408.
[33] Li K, Luo H, Huang L, Luo H and Zhu X. Microsatellite instability: a review of what the oncologist should know. Cancer Cell Int 2020; 20: 16.
[34] Yan C, Niu Y, Ma L, Tian L and Ma J. System analysis based on the cuproptosis-related genes identifies LIPT1 as a novel therapy target for liver hepatocellular carcinoma. J Transl Med 2022; 20: 452.

[35] Uzbekov R and Prigent C. A journey through time on the discovery of cell cycle regulation. Cells 2022; 11: 704.
[36] Bhosale PB, Abusaliya A, Kim HH, Ha SE, Park MY, Jeong SH, Vetrivel P, Heo JD, Kim JA, Won CK, Kim HW and Kim GS. Apigetrin promotes TNFα-induced apoptosis, necroptosis, G2/M phase cell cycle arrest, and ROS generation through inhibition of NF-κB pathway in Hep3B liver cancer cells. Cells 2022; 11: 2734.
[37] Zhan L, Huang C, Meng XM, Song Y, Wu XQ, Miu CG, Zhan XS and Li J. Promising roles of mammalian E2Fs in hepatocellular carcinoma. Cell Signal 2014; 26: 1075-1081.
[38] Bejarano L, Jordão MJC and Joyce JA. Therapeutic targeting of the tumor microenvironment. Cancer Discov 2021; 11: 933-959.
[39] Lee YH, Chuah S, Nguyen PHD, Lim CJ, Lai HLH, Wasser M, Chua C, Lim TKH, Leow WQ, Loh TJ, Wan WK, Pang YH, Soon G, Cheow PC, Kam JH, Iyer S, Kow A, Bonney GK, Chan CY, Chung A, Goh BKP, Zhai W, Chow PKH, Albani S, Liu H and Chew V. IFNγ(-)IL-17(+) CD8 T cells contribute to immunosuppression and tumor progression in human hepatocellular carcinoma. Cancer Lett 2023; 552: 215977.
[40] Faggioli F, Palagano E, Di Tommaso L, Donadon M, Marrella V, Recordati C, Mantero S, Villa A, Vezzoni P and Cassani B. B lymphocytes limit senescence-driven fibrosis resolution and favor hepatocarcinogenesis in mouse liver injury. Hepatology 2018; 67: 1970-1985.
[41] Fang T, Lv H, Lv G, Li T, Wang C, Han Q, Yu L, Su B, Guo L, Huang S, Cao D, Tang L, Tang S, Wu M, Yang W and Wang H. Tumor-derived exosomal miR-1247-3p induces cancer-associated fibroblast activation to foster lung metastasis of liver cancer. Nat Commun 2018; 9: 191.
[42] Trehanpati N and Vyas AK. Immune regulation by T regulatory cells in hepatitis B virus-related inflammation and cancer. Scand J Immunol 2017; 85: 175-181.
[43] Rui R, Zhou L and He S. Cancer immunotherapies: advances and bottlenecks. Front Immunol 2023; 14: 1212476.

**Table S1.** List of primer sequences for Reverse Transcription Quantitative Polymerase Chain Reaction (RT-qPCR) and sequences for siRNAs

| Primers | | Sequence (5'-3') |
|---|---|---|
| ZNF248 | Forward | TTGGAAATGGAGCCGTATGGA |
| | Reverse | CCCAGGTTTTGTCACTCACTTTA |
| GAPDH | Forward | AATGGGCAGCCGTTAGGAAA |
| | Reverse | GCCCAATACGACCAAATCAGAG |
| siRNAs | | Sequence (5'-3') |
| si-NC | Forward | GACUGACUCCCGUGUAAGGACUCAA |
| | Reverse | UUGAGUCCUUACACGGGAGUCAGUC |
| si-ZNF248-1 | Forward | GACUCCAGUCCCUUGUGGGAAACAA |
| | Reverse | UUGUUUCCCACAAGGGACUGGAGUC |
| si-ZNF248-2 | Forward | ACUCCAGUCCCUUGUGGGAAACAAU |
| | Reverse | AUUGUUUCCCACAAGGGACUGGAGU |
| si-ZNF248-3 | Forward | CAGUCCCUUGUGGGAAACAAUCCCU |
| | Reverse | AGGGAUUGUUUCCCACAAGGGACUG |

**Table S2.** Antibodies used in this study

| Antigens | Manufacturers | Application |
|---|---|---|
| GAPDH | #5174, Cell Signaling Technology, Beverly, MA, USA | 1:1000 for WB |
| Anti-rabbit IgG HRP conjugated | #7074, Cell Signaling Technology, Beverly, MA, USA | 1:1000-1:3000 for WB |
| Anti-mouse IgG HRP conjugated | #7076, Cell Signaling Technology, Beverly, MA, USA | 1:1000-1:3000 for WB |
| ZNF248 | #PA5-31967, Invitrogen, Waltham, MA | 1:1000 for WB |
| BrdU | ab2284, ABCAM, Cambridge, UK | 5 μg per test |
| AKT | #AF6261, Affinity Biosciences, Cincinnati, OH, USA | 1:500-1:2000 for WB |
| p-AKT (Ser473) | #AF0016, Affinity Biosciences, Cincinnati, OH, USA | 1:500-1:2000 for WB |
| PI3K | #AF5112 Affinity Biosciences, Cincinnati, OH, USA | 1:500-1:2000 for WB |
| p-PI3K | #AF4369, Affinity Biosciences, Cincinnati, OH, USA | 1:500-1:2000 for WB |

WB, Western Blot.